Niobium Fermi surface and the magnetoacoustic interaction: Polarization selectivity*

J. R. Leibowitz and G. V. Blessing†
Department of Physics, Catholic University, Washington, D. C.

E. M. Alexander
U. S. Naval Research Laboratory, Washington, D. C.

(Received 10 September 1973)

The magnetoacoustic interaction for field $\vec{H}$ normal to propagation vector $\vec{q}$ has been studied in high-purity niobium at frequencies extending to 650 and 430 MHz for longitudinal and transverse waves, respectively. Fermi-surface calipers determined for $\vec{q} \| [100]$ and $\vec{\epsilon} \| [010]$ agree within about 2% with the augmented-plane-wave theoretical values for the distorted ellipsoids. Also, an interesting and useful "caliper-selectivity" mechanism operative in the transverse-wave case was observed which, for particular orientations of wave polarization $\vec{\epsilon}$, served to isolate individual calipers so that the calipers corresponding to a single Fermi sheet were swept out as $\vec{H}$ was rotated through 360°. The corresponding presence of a single period in the oscillations at all field angles permitted relaxation of the number of oscillations required for precise determination of the electron momenta.

INTRODUCTION

We have recently reported[1,2] observation of magnetoacoustic (MA) oscillations in niobium. Preliminary results on the caliper momenta for the "distorted ellipsoids" were given, and evidence shown[1] for a caliper-selectivity effect in the MA interaction determined by polarization orientation. In the present work these effects are explored using high-purity Nb (residual resistance ratio ~ 5000) and acoustic frequencies extending to 650 and 430 MHz for longitudinal and transverse waves, respectively. Values of ql to about 30 were attained under the conditions of these MA experiments. (In this paper we refer only to MA effects corresponding to field $\vec{H}$ perpendicular to wave propagation vector $\vec{q}$.) The Fermi-surface calipers determined from the MA oscillations for directions in the (100) plane agree within 2% with the dimensions of the distorted ellipsoids determined from the augmented-plane-wave (APW) calculations of Mattheiss.[3] The present data permit further comment on the nature of the caliper-selectivity effect determined by polarization orientation.

It has for some time been recognized that the MA technique is generally a less useful tool for Fermiology than, for example, the de Haas–van Alphen method, owing primarily to the fact that the MA technique imposes a relatively severe specimen-purity constraint for the observation of N oscillations of a given oscillation sequence. The availability of a relatively small number of oscillations can, of course, be a serious liability when several oscillation periods (corresponding to several independent contributions from a complex Fermi surface) are present simultaneously in the data; Fourier decomposition becomes formidable, if not impossible, when N is small and there are several periods present in the data. The aforementioned limitation on the MA technique is unfortunate since MA oscillations are often relatable to Fermi-surface caliper dimensions.

The present work indicates, however, that under appropriate conditions the transverse wave interacts more selectively than the longitudinal with electrons at the available caliper end points, with the effect that the anticipated mixing of periods is suppressed in the MA oscillations. In these instances, the introduction of a shear polarization serves to simplify rather than complicate data analysis: the reduction or removal of interference in the observed MA oscillations relaxes the ql constraint, since the number of oscillations N required for the determination of a Fermi-surface caliper to given precision is now reduced. We are reminded (cf. Ref. 4) that N is a function of ql and $\omega\tau$.

It has already been noted that when several Fermi-surface extremal calipers obtain for a given wave and field orientation it is expected that the associated sequences of MA oscillations—each sequence corresponding in general to a given extremal Fermi-surface caliper (when extremal orbits dominate)—will produce a complex superposition in the observed oscillations. The relative amplitude of the nth oscillation from a given sequence will, in the case of an arbitrary Fermi surface, depend on a number of factors[4,5] including the Fermi-surface curvatures (along and normal to the cyclotron orbit) evaluated at the appropriate caliper end point. As we shall see below, for the case of a transverse wave the oscillation amplitudes are weighted, in addition, by the orientation of the wave polarization vector $\vec{\epsilon}$ relative to the Fermi surface. The experimental data found in the pres-

ent work demonstrate that, when both $\vec{q}$ and $\vec{\epsilon}$ are along ⟨100⟩ directions in niobium, only a single Fermi sheet, one of the distorted ellipsoids, contributes significantly to the observed oscillations.

Comparison[1,2] of the experimental data from longitudinal waves having $\vec{q} \parallel [100]$, and transverse waves having $\vec{q} \parallel [100]$ both with $\vec{\epsilon} \parallel [010]$ and [011], demonstrates the strong influence of shear-polarization orientation on caliper selectivity. The extremal calipers, determined for all directions of magnetic field $\vec{H}$ in the (100) plane swept in 10° intervals, agree within about 2% (see below) with those derived for the distorted ellipsoids from the APW calculations of Mattheiss.[3] The high precision with which extremal calipers were determined was made possible by the fact that, for every field orientation in the case $\vec{q} \parallel [100]$ and $\vec{\epsilon} \parallel [010]$, only one oscillation period contributed significantly to the observed transverse-wave attenuation α_t versus reciprocal magnetic field H^{-1}. This is in sharp contrast to the longitudinal-wave data, for which strong interference was evident in the MA oscillations at every sampled orientation of acoustic wave and magnetic field.

EXPERIMENTAL METHOD

The pulse-transmission technique was used. AC-cut quartz piezoelectric transducers were bonded to both ends of the acoustic path, consisting of the sample and AC-cut quartz time-delay rod. The samples were in the form of oriented single-crystal circular disks of niobium having base diameters of about 5 mm and thicknesses ranging from about 0.5 to 1.5 mm, depending on crystal orientation. The acoustic probe provided for remote tuning of trimmer capacitors in L-C matching circuits placed in the sample holder just before each of the transducers. The circuits each consisted of a variable trimmer capacitor (2–100 pF) in series with the center coaxial cable, and a variable inductive loop to ground which was necessarily preset before insertion of the probe into the Dewar. Temperature in the hermetically sealed sample chamber was recorded by a germanium thermometer and controlled by adjustment of helium gas pressure in the chamber and current to a wire-wound heater on the sample holder.

The MA measurements were made at constant temperature set at values between 6 and 7 °K while magnetic field $\vec{H}$, oriented in the plane normal to propagation vector $\vec{q}$ and provided by a rotatable Varian electromagnet, was swept to 12 kOe. The operating temperature was chosen to be sufficiently low to minimize the effects of oscillation damping due to thermal phonon-electron scattering, and yet not so low as to require excessive applied field in order to exceed the superconducting upper critical field H_{c2}; it was necessary to keep H_{c2} sufficiently small to permit observation of the low-field MA oscillations. These rather unusual constraints in applying the MA technique to niobium are attributable to the fact that Nb has the highest transition temperature among the elements, and the electronic attenuation of the acoustic waves is strongly phonon limited near T_c.

FERMI SURFACE OF NIOBIUM

Since niobium is body-centered cubic, its first Brillouin zone is a dodecahedron. Niobium is a transition metal with five conduction electrons per atom, four from the unfilled d band and one from the s band. The Fermi surface is by now reasonably well understood. The APW calculations of Mattheiss[3] and the experimental observations[6,7] are in rather good agreement. The first Brillouin zone is completely filled, the second almost filled, and the third about 50% filled. Figure 1 shows the Fermi-surface structure together with the Brillouin zone (after Mattheiss[3]). In the second reduced zone, centered on point Γ, is an eight-armed closed surface (which, following convention, will be referred to as the octahedron). In the third zone, which contains the remainder of the Fermi surface, and a multiply connected "jungle-gym" structure and twelve "distorted ellipsoids" bisected by the faces of the Brillouin zone. Following standard notation, the point Γ labels the center of the zone, points N indicate the center of each face of the dodecahedron, and points P and H label the corners of threefold and fourfold symmetry, respectively, on the zone boundary. Note that the "arms" of the jungle gym extend outward from Γ along all of the ⟨100⟩ directions to the zone corners H. The second-zone surface, the octahedron, is partially degenerate with the jungle gym. While all of the twelve ellipsoids are, of course, equivalent, it will prove useful to separate them into two groups: The ellipsoids bisected by the (100)

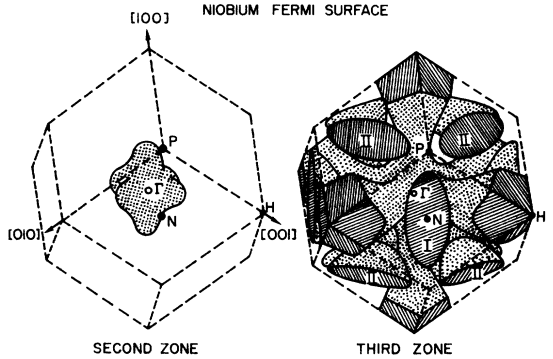

FIG. 1. Hole sheets of the Fermi surface in the second and third Brillouin zones of niobium [after Mattheiss (Ref. 3)].

central plane will be called type-A ellipsoids while the remainder will be referred to as type-B.

From the APW calculations of Mattheiss[3] we determined the effective zones of the niobium Fermi sheets corresponding to principal wave-propagation directions in the niobium crystal. The effective zones are the loci on the Fermi surface for which the surface normals are perpendicular to $\vec{q}$, i.e., the paths satisfying $\vec{q}\cdot\vec{v}_F = 0$ (v_F is the Fermi velocity). The effective zones for the case $\vec{q} \parallel [100]$ are shown projected onto the (100) plane in Fig. 2, where the indicated k values are given in reciprocal angstroms. It is necessary to take the projection indicated in Fig. 2 since the extremal calipers measured in the transverse MA effect ($\vec{H} \perp \vec{q}$) are perpendicular to $\vec{q}$ in $\vec{k}$ space; for these projected effective zones, the extremal diameters perpendicular to the field direction [swept in the (100) plane] are the calipers measured by the MA effect (cf. Ref. 5). In Fig. 2 the effective zone of the octahedron is the four-armed star-shaped figure centered on Γ; the jungle-gym effective zones correspond (i) to the larger four-armed figure centered at Γ and extending to the zone faces, and (ii) to the circle centered at Γ; and the effective zones of the type-A ellipsoids are the figures labeled I and II. For all the figures discussed so far, the effective zones are simply the intersection of the given Fermi sheet with the (100) plane [or, for the case of the circle centered on Γ, a plane displaced from but parallel to (100)]. For the type-B ellipsoids the effective zones are not determined quite so simply, since the ellipsoids are tilted relative to the (100) plane (see Fig. 1) with the consequence that the effective zones do not lie in a plane parallel to (100). (In point of fact, they are not planar.) To obtain the calipers for the type-B ellipsoids, therefore, it was necessary to take the projections of the effective zones in the (100) plane. This was found to be most readily accomplished from a three-dimensional model of a distorted ellipsoid, the construction of which was guided by unpublished computations of Matthiess. The effective zones were then determined and their projections transferred mechanically to one (100) plane. These projections are labeled III–VI. Figure 2 permits direct determination of the theoretical values for the extremal calipers measured by the MA effect for the case $\vec{q} \parallel [100]$ and any given orientation of $\vec{H}$ in the (100) plane.

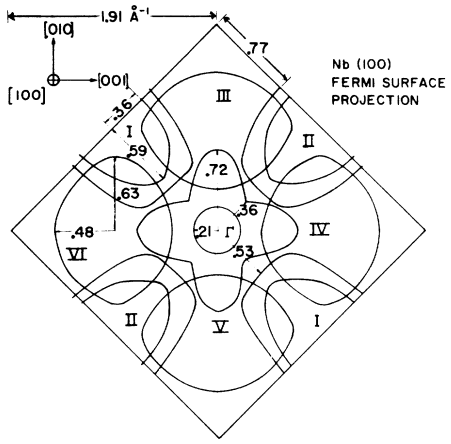

FIG. 2. Effective zones of niobium projected onto the (100) plane and corresponding to $\vec{q} \parallel [100]$. Units are reciprocal angstroms (Å^{-1}).

MAGNETOACOUSTIC ATTENUATION: OSCILLATION AMPLITUDE

Let us examine factors determining the amplitudes of oscillations associated with a given Fermi-surface caliper. Mertsching[4] has derived an expression for the longitudinal wave MA attenuation which is of considerable interest here. The attenuation for longitudinal waves, for the case $\vec{H} \perp \vec{q}$ and arbitrary Fermi surfaces is

$$\alpha_L = C\left(\left(\frac{2\pi}{q\,|\partial^2 D/\partial k_z^2|}\right)^{1/2} \times \frac{m_c \Lambda_l}{|\partial v_l/\partial\Theta|}\,\frac{\cos(qD-\frac{3}{4}\pi)}{\sinh(\pi/\omega_c\tau)}\right)_{\vec{q}\cdot\vec{v}=0} \cdot \quad (1)$$

Here only the oscillatory term in the MA attenuation is given. Equation (1) represents a limiting form applicable to the case in which (i) Fermi-surface calipers are associated with extremal orbits, and (ii) it is assumed that the cyclotron orbits in $\vec{k}$ space are closed and have two symmetric points of stationary phase. We shall infer from the data that these assumptions are not unreasonable for the present case, since the MA oscillations are found (see later) to be assignable to the distorted ellipsoids. The simplified form represented by Eq. (1) also contains the assumptions of constant electron relaxation time τ and $ql \gg 1$. In Eq. (1), D is the distance between planes of constant phase in the closed orbit (in a plane normal to $\vec{H}$), k_z is the component of $\vec{k}$ along $\vec{H}$, m_c is the cyclotron mass, Λ_l is the longitudinal-wave deformation potential, $v_l = \hat{q}\cdot v_F$ (where v_F is the Fermi velocity), θ is the polar angle in the orbital plane, and $\omega_c = eH/m_c C$ is the cyclotron frequency. Equation (1) indicates explicitly the effect on oscillation amplitude of the factors $|\partial^2 D/\partial k_z^2|$ and $|\partial v_l/\partial\theta|$, which are directly relatable to Fermi-surface curvatures at the caliper end points.

The expression for the amplitude of the oscillations in Eq. (1) may be readily understood physically[6] when it is noted that the factor $[2\pi/(q|\partial^2 D/\partial k_z^2|)]^{1/2}$ represents the width in k space of the band of cyclotron orbits effectively contributing to

the interaction, while the amplitude factor $|\partial v_l/\partial\theta|^{-1}$ is relatable to the time which an orbiting electron spends in a region of nearly constant phase of the acoustic wave. Correspondingly, these two factors are relatable, respectively, to the following radii of curvature evaluated at the given caliper end point: (i) along the intersection with the plane normal to the cyclotron orbit, and (ii) along the effective zone. These assertions are readily demonstrated. Taking $\vec{H}$ to be in the z direction, we have to first order

$$D(k_z) - D_{\max} = \tfrac{1}{2}(\Delta k_z)^2 \frac{\partial^2 D}{\partial k_z^2}.$$

And since the maximum value of $[D(k_z) - D_{\max}]$ for which electron orbits will constructively contribute to the attenuation is about $\frac{1}{2}\lambda$ we find, following Mertsching, [4] that the effective band of cyclotron orbits is

$$\Delta k_z \approx \left(\frac{2\pi}{q\,|\partial^2 D/\partial k_z^2|}\right)^{1/2}_{D_{\max}}.$$

Note that the radius of curvature for a point at $D_{\max}$ is simply $|\partial^2 D/\partial k_z^2|^{-1}$. Now consider the factor $m_c/|\partial V_l/\partial\theta|$. Since the curvature $\vec{\kappa}$ may be defined as $\vec{\kappa} = d\vec{T}/ds$, where $\vec{T}$ is the unit tangent and ds is an element of arc, we may write approximately

$$\frac{m_c}{|\partial v_l/\partial\theta|} = \frac{m_c}{(v_l/\omega_c)(1/R)(dk/dt)} = \frac{R\hbar}{v_l v_F},$$

where R is the radius of curvature along the cyclotron orbit and evaluated at the given point. Since v_l is smallest on the effective zone (the locus satisfying $\vec{v}_F \cdot \vec{q} \approx 0$) it is evident that the factor $|\partial v_l/\partial\theta|^{-1}$ roughly "measures" the time the electrons spend near planes of constant phase of the acoustic wave.

From the foregoing it is evident that the amplitude factors which we have so far considered are also applicable to the transverse-wave interaction, since they represent the physically reasonable assertion that the amplitude of the nth oscillation depends on the width of the band of cyclotron orbits which contribute and the time spent by the orbiting electrons on planes of constant phase. At the same time Eq. (1) provides an even qualitatively incomplete criterion for MA oscillation amplitudes in the case of transverse waves, since it completely neglects the effect of wave polarization orientation.

TRANSVERSE-WAVE INTERACTION; POLARIZATION SELECTIVITY

Our purpose here is to indicate the nature of the caliper selectivity attributable to the orientation of the wave polarization vector $\vec{\epsilon}$. It then becomes possible to understand how it may happen that, in the present data for $\vec{q} \parallel [100]$ and $\vec{\epsilon} \parallel [010]$, calipers corresponding essentially to a single Fermi sheet are "swept out" as field $\vec{H}$ is rotated through 360°. Pippard[5] has treated the transverse MA attenuation ($\vec{H} \perp \vec{q}$) for the case of arbitrary Fermi surfaces and transverse as well as longitudinal waves. It is necessary to take into consideration that the forces of interaction between electrons and lattice, the Fermi velocity $\vec{v}_F$, and the relaxation time τ are all variable over a given cyclotron orbit. It is no surprise, therefore, that the final forms of Pippard's MA attenuation expressions, which include the nonoscillatory contributions [see Eqs. (47) and (48) in Ref. 5], are very complex—even when $\vec{H}$, $\vec{q}$, and $\vec{\epsilon}$ are restricted to directions of high lattice symmetry—and not best suited to displaying the role of $\vec{\epsilon}$ orientation on amplitudes of a given set of oscillations. But, for this purpose, it is sufficient to note that the attenuation may be written

$$\alpha = (4\pi^3\hbar M v_s u^2)^{-1} \int \frac{|\Delta\epsilon|^2}{l}\, dS, \tag{2}$$

where M is the density of the metal, v_s and u are the acoustic wave and particle velocities respectively, $|\Delta\epsilon|$ is the energy displacement of the Fermi surface, and l is the electron mean free path. In turn, the displacement of the Fermi surface due to force component π parallel to the electron motion is of the form

$$\Delta\epsilon(0) = \int_{-\infty}^{0} v\pi \exp\left(-\int_t^0 \frac{dt}{\tau}\right) dt. \tag{3}$$

Here $\Delta\epsilon(0)$ is the displacement due to all events up to time $t = 0$. Thus, we see that $|\Delta\epsilon|^2$ appears as a factor in the integrand of the surface integral determining α, and, in turn, the force component π appears linearly as a factor in the integral determining the Fermi-surface displacement $\Delta\epsilon$. From Eqs. (2) and (3), therefore, it is clear that, when it is sufficient for qualitative analysis to ignore variation of the magnitude of the Fermi velocity and relaxation time on the cyclotron orbits of a given Fermi sheet, the oscillation amplitudes are determined roughly by $|\pi|^2$. In point of fact, we find that this criterion seems to be of crucial importance in determining the shear-wave oscillation amplitudes, and generally quite overwhelms that based on Fermi-surface curvatures, referred to in the preceding section. Note that $\vec{\epsilon}$ orientation has been shown, in experimental studies[9,10] on copper, to be important in the open-orbit oscillations as well.

Let us now consider the forces associated with displacements $\Delta\epsilon$. In the free-electron problem it is possible to determine the attenuation by treating the electric and magnetic fields coupling the separate electron and lattice assemblies. This separation is harder to achieve in the case of ar-

bitrary Fermi surfaces. In Pippard's treatment of the interaction of acoustic waves with an arbitrary Fermi surface, the lattice is taken to be stationary and the fictitious forces which arise are then described. Each of these forces is associated with an electronic current relative to the lattice. If in the transverse-wave problem the current-balance condition $\vec{J}_{ion}+\vec{J}_{el}=0$ is assumed to hold, then the electric field is determined to be that necessary to guarantee no net electronic current relative to the lattice. The forces associated with the electron-acoustic wave interaction are found to be of the following form:

$$\pi_1 = iq\hbar\vec{K}\cdot\vec{u}, \tag{4a}$$

$$\pi_2 = iq\hbar\vec{k}\cdot\vec{u}\sin\theta\cos\phi, \tag{4b}$$

and

$$F_E = e\vec{E}\cdot\vec{v}_F/v_F, \tag{4c}$$

where π_1 is associated with Fermi-surface deformation, π_2 is another fictitious force which arises in the stationary-lattice problem (labeled by Pippard the "relative-velocity" force), and F_E is that attributable to the electric field insuring current balance. In Eqs. (4), $\vec{K}$ is a Fermi surface deformation parameter (variable over the Fermi surface) defined by the relation $dk_n=\vec{K}\cdot\vec{w}$, where $\vec{w}$ is the strain and dk_n is the normal shift of the Fermi surface; $\vec{v}_F$ is the Fermi velocity; θ is the angle enclosed by $\vec{v}_F$ and the z axis of the given coordinate system (which axis is also taken to be along the direction of the applied magnetic field $\vec{H}$); and ϕ is the angle enclosed by the x axis (taken to be the direction of the wave propagation vector $\vec{q}$) and the projection of $\vec{v}_F$ in the x-y plane. It is to be noted that Eqs. (4) give the components of the forces along the direction of electron motion, i.e., along $\vec{v}_F$, since these are the components responsible for the shift $\Delta\epsilon$ of the Fermi surface and therefore the electronic attenuation. Accordingly, we note in Eq. (4c), it is not the electric field $\vec{E}$ which is of interest, but rather its component in the direction of electron motion.

It should be noted that in the free-electron model[11,12] the MA oscillations depend on relative orientation of $\vec{H}$ and $\vec{\epsilon}$; v_F at caliper end points is always normal to $\vec{H}$. But in the case of a real metal $\vec{v}_F\cdot\vec{\epsilon}$ is the relevant parameter, and it will be finite, in general, even for the case $\vec{\epsilon}\parallel\vec{H}$.

DATA AND ANALYSIS

Elsewhere[1,2] we reported MA results which compared the longitudinal and transverse MA oscillations and gave preliminary transverse-wave caliper determinations. We found for the case of 510-MHz longitudinal waves having $\vec{q}\parallel[100]$ that the oscillations suffered strong harmonic mixing, to the extent that periodicity in $1/H$ was partially obscured. The observed sensitivity of the oscillation pattern to small changes of $\vec{H}$ orientation in the (100) plane (cf. Fig. 1 of Ref. 2) was consistent with the assertion that several calipers were represented here. In contrast the comparable case (comparable q value) for the case of 210-MHz transverse waves gave very different results.[2] For $\vec{q}\parallel[100]$, $\vec{\epsilon}\parallel[010]$ the transverse-wave oscillations were periodic in $1/H$; for each orientation of $\vec{H}$ relative to $\vec{\epsilon}$ a single period was dominant.[1,2] A selectivity determined by $(\hat{v}_F\cdot\hat{\epsilon})$ in the transverse-wave MA interaction was inferred from the results. In the present work the transverse-wave data is examined in more detail and at higher frequencies in an attempt to gain insight into the nature of the transverse MA interactions in a multisheet Fermi surface such as that of Nb.

$$\vec{q}\parallel[100], \vec{\epsilon}\parallel[010]$$

For this wave orientation MA oscillations were obtained for applied magnetic field varied, in 10° steps, through 360° (in the plane perpendicular to $\vec{q}$). Figures 3–6 show representative traces, corresponding to $\vec{H}\parallel\vec{\epsilon}$, H 35° from $\vec{\epsilon}$, H 65° from $\vec{\epsilon}$, and $\vec{H}$ 90° from $\vec{\epsilon}$ (i.e., $\vec{H}\perp\vec{\epsilon}$), respectively. (Actually $\vec{H}$ was misaligned by about 5° from parallel to $\vec{\epsilon}$ and perpendicular to $\vec{\epsilon}$ in Figs. 3 and 6,

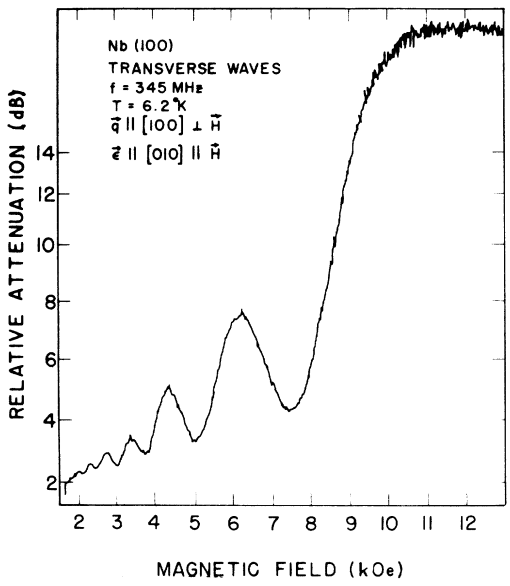

FIG. 3. Nb (100) magnetoacoustic oscillations: α_N vs H for $\vec{\epsilon}\parallel[010]\parallel\vec{H}$. [Actually, curve is mislabeled; $\vec{\epsilon}$ found to be 5° from direction parallel to H].

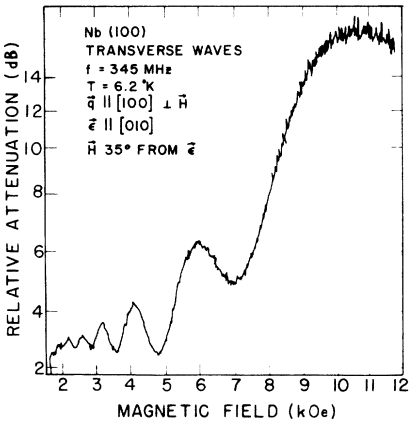

FIG. 4. Nb (100) magnetoacoustic oscillations: α_N vs H for $\vec{\epsilon} \parallel [010]$ and 35° from $\vec{H}$.

respectively.) These data were taken at a temperature of 6.2 °K and a frequency of 345 MHz, which conditions permitted observation of a maximum of seven oscillations in the attenuation patterns.

We find that for the case labeled $\vec{H} \parallel \vec{\epsilon}$ there is no evidence in the MA oscillations for mixing of periods; for the case labeled $\vec{H} \perp \vec{\epsilon}$ some evidence for mixing may be inferred from the shape of the oscillation envelope. For all field angles each set of MA oscillations was found to be well represented by a single period in α vs $1/H$. A polar plot of the corresponding extremal calipers is shown in Fig. 7. In the free-electron problem[11,12] the rotation of $\vec{H}$ relative to $\vec{\epsilon}$ affects the amplitude of oscillations but not the period: the extremal caliper Δk is the diameter (constant) of the free-electron sphere; and the changing amplitude merely reflects the changing orientation of Fermi velocity $\vec{v}_F$ relative to field $\vec{E}$ coupling the electrons and lattice. In the real metals case, however, as

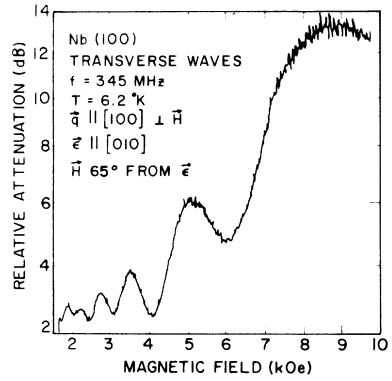

FIG. 5. Nb (100) magnetoacoustic oscillations: α_N vs H for $\vec{\epsilon} \parallel [010]$ and 65° from $\vec{H}$.

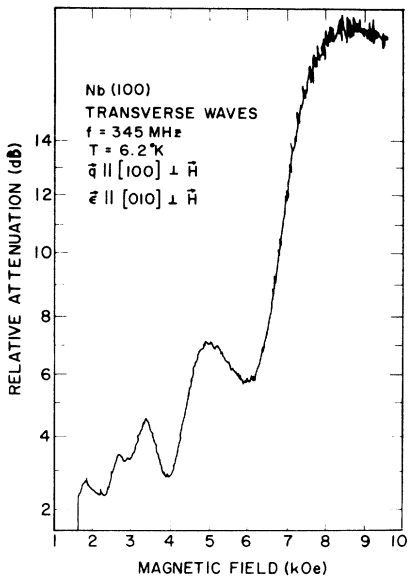

FIG. 6. Nb (100) magnetoacoustic oscillations: α_N vs H for $\vec{\epsilon} \parallel [010]$, $\vec{\epsilon} \perp \vec{H}$. [Actually, curve is mislabeled; $\vec{\epsilon}$ found to be 5° from direction perpendicular to $\vec{H}$.

Eqs. (2)–(4) predict and as the present experimental results show, the orientation of $\vec{\epsilon}$ with respect to $\vec{v}_F$ can affect not only the amplitude of oscillations but the period as well. Note that the polar plot has twofold rotational symmetry. This is in sharp contrast to the case for longitudinal waves having $\vec{q} \parallel [100]$, for which the MA oscillations must reflect fourfold rotational symmetry with respect to field direction in the (100) plane of Nb.

Making use of the reflection symmetry about the principal axes, the Δk values represented in Fig. 7 were folded into one quadrant, as shown (open circles) in Fig. 8. The solid line represents the theoretical extremal caliper dimension as a function of field angle for the distorted ellipsoid (III, V) in Fig. 2. Note that, for all field orientations, the experimental Δk values agree within 2% with the theoretically determined calipers for ellipsoids (III, V). We shall see further evidence later for this ellipsoid (III, V) selectivity of the transverse-wave MA interaction, when we review the data obtained for $\vec{q} \parallel [100]$ and $\vec{\epsilon} \parallel [011]$.

This is a most striking result. As Fig. 2 shows, for any given orientation of field in the (100) plane a number of extremal calipers are available: the figure gives those projections of the Fermi sheets such that in the case $\vec{q} \parallel [100]$ and for any given orientation of $\vec{H}$ in the (100) plane [the plane of the figure], the extremal calipers corresponding to MA oscillations are those normal to $\vec{H}$. Let us admit, for the present, the possibility that for the case $\vec{q} \parallel [100]$ cyclotron orbits on sheets other than

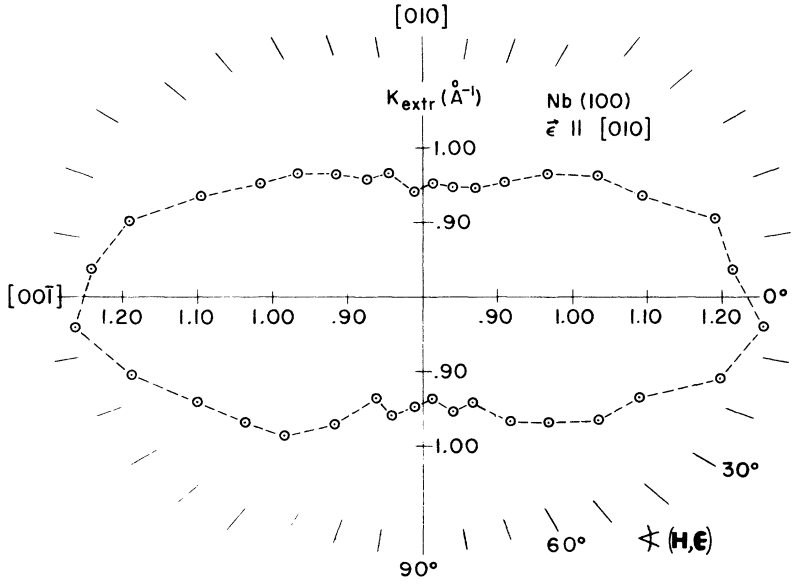

FIG. 7. Nb (100) polar plot of Δk vs angle $(\vec{H}, \vec{\epsilon})$ for $\vec{\epsilon} \parallel [010]$.

the ellipsoids are relatively unfavorable as contributors to the observed MA oscillations. Further, let us tentatively reject contributions from the type-A ellipsoids [ellipsoids labeled I in Fig. 1 and labeled I and II in Fig. 2, i.e., those ellipsoids bisected by the (100) plane]. It remains to account for the surprising further discrimination implied in Fig. 8. For that result implies it is possible to distinguish among the ellipsoids of type B, so as to discriminate against ellipsoids (IV, VI) in favor of (III, V)! In point of fact, such a distinction would in the case of longitudinal waves along [100] violate symmetry requirements.

The effect of the Fermi-surface curvatures at caliper end points on oscillation amplitude is insufficient of itself to account for the observations, since it cannot lead to the observed reduction of the fourfold symmetry. However, the polarization selectivity discussed in the last section is capable of accounting for the twofoldedness observed in Fig. 8. In light of Eqs. (2)–(4) we examine the rough amplitude criterion $|\hat{\epsilon} \cdot \hat{v}_F|^2$, where $\hat{\epsilon}$ is the unit vector in the direction of the wave polarization. Table I lists for each field angle (measured with reference to $\vec{\epsilon}$) the values of $(\hat{\epsilon} \cdot v_F)^2$ measured at caliper end points, together with the corresponding extremal caliper values. Note that for every angle for which there is experimental data $(\hat{\epsilon} \cdot v_F)^2$ is larger—significantly larger at most angles—for the (III, V) ellipsoids than for (IV, VI). And for every field angle, the experimental caliper values are, as we've already seen, in excellent agreement with the theoretical Δk values corresponding to ellipsoids (III, V).

The increasing influence of a second oscillation period (corresponding to a second caliper) with increase of angle made by $\vec{H}$ relative to $\vec{\epsilon}$ is demonstrated in Figs. 3–6; the evidence for harmonic mixing in the oscillation envelopes becomes significant as $\vec{H}$ approaches 90° relative to $\vec{\epsilon}$ (column 7 of Table I summarizes observations). At the same time, the difference between the $(\hat{\epsilon} \cdot \hat{v}_F)^2$ values of columns 2 and 4 become smaller as $\vec{H}$ approaches 90°. The relatively unimportant role of Fermi-surface curvatures on MA amplitudes would appear to be demonstrated here: The curvature coefficients in Eq. (1) are roughly five times greater when $\vec{H} \perp \vec{\epsilon}$ for the (IV, VI) ellipsoids than for (III, V). (We are reminded of the qualitatative nature of this comparison. For example, we cannot quantitatively compare the effect of shear deformation potential in Nb on relative amplitudes.)

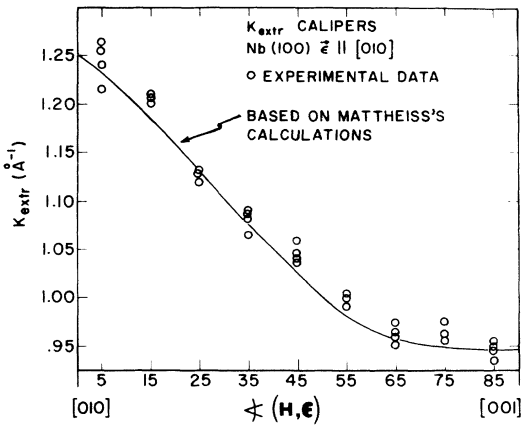

FIG. 8. Δk vs angle $(\vec{H}, \vec{\epsilon})$ for $q \parallel [100]$, $\vec{\epsilon} \parallel [010]$. Experiment vs theory for ellipsoid (III, V).

TABLE I. Δk theoretical and experimental values for Nb (100), $\vec{\epsilon} \parallel [010]$. Δk is given in units of Å^{-1}.

	Theory				Experiment	
1	2	3	4	5	6	7
$(\vec{H}, \vec{\epsilon})$	$(\hat{\epsilon} \cdot \hat{v}_F)^2$ (IV and VI)	Δk	$(\hat{\epsilon} \cdot \hat{v}_F)^2$	Δk (III and V)	Δk	mixing
0°	0	0.94	0	1.25 Å^{-1}	(Data not available)	
5°	0	0.94	0.1	1.23	1.24 Å^{-1}	negligible
15°	0.1	0.95	0.3	1.19	1.21	negligible
25°	0.1	0.96	0.4	1.13	1.13	negligible
35°	0.1	0.98	0.6	1.08	1.08	negligible
45°	0.2	1.03	0.8	1.03	1.04	negligible
55°	0.4	1.08	0.9	0.98	1.00	(present
65°	0.6	1.13	0.9	0.96	0.96	in
75°	0.7	1.19	0.9	0.95	0.96	increasing
85°	0.9	1.23	1.0	0.94	0.95	amounts)
90°	1.0	1.25	1.0	0.94	(Data not available)	

$\vec{q} \parallel [100], \vec{\epsilon} \parallel [011]$.

The data from this wave orientation support the above observations. The results are consistent with $(\hat{v}_F \cdot \hat{\epsilon})^2$ as a rough scaling criterion in caliper selectivity. Further, these data support the conclusion that only ellipsoids of type B are significant in the MA interaction for $\vec{q} \parallel [100]$.

For the new wave orientation, $\vec{q}$ still parallel to [100] but $\vec{\epsilon}$ rotated 45° and aligned parallel to a ⟨110⟩ direction, the ultrasonic frequency used was 375 MHz (as compared with 345 MHz for $\vec{\epsilon} \parallel [010]$). Otherwise, the experimental conditions were the same. The value of gl was expected to be comparable (~ 30), an expectation supported by observation of the same number of oscillations in the attenuation patterns, i.e., $N = 7$, as demonstrated by Fig. 9. The change of polarization orientation causes a dramatic change in the polar plot of observed Δk values and gives additional evidence for the selectivity exerted by $\vec{\epsilon}$ orientation.

As we see from Table II, the $(\hat{\epsilon} \cdot \hat{v}_F)^2$ criterion now fails to select either set of ellipsoids consistently; as may be seen from columns 2 and 4 its values are comparable for ellipsoids (IV, VI) and (III, V) for almost the entire range of field angles. However, from Fig. 2 we can see that for the present case, $\vec{\epsilon} \parallel [011]$, the type-$B$ ellipsoid calipers both for $\vec{H} \parallel \vec{\epsilon}$ and $\vec{H} \perp \vec{\epsilon}$ are degenerate. That is, the Δk values for ellipsoids (IV, VI) and (III, V) are the same at those field orientations. Hence, if only the type-B ellipsoids are important in the MA interaction, no mixing should be apparent in the observed oscillations at these field angles, and the observed period should be about 1.03 Å^{-1}. That these are precisely the results observed may be seen in Fig. 9 and Table II. Figure 10, which shows MA oscillations for the case $\vec{H}$ 40° from $\vec{\epsilon}$, illustrates the strong mixing observed when $\vec{H}$ orientation is not near either 0° or 90° relative to $\vec{\epsilon}$. In contrast, note the relatively unmixed oscillations of Fig. 9; the upper and lower curves show the same period, as required. The actual amplitudes differ, of course, since the electric field component along $\vec{v}_F$ is far greater for the lower curve (see Table II).

It is to be emphasized that the data for the present orientation, $\vec{q} \parallel [100]$ and $\vec{\epsilon} \parallel [011]$, are consistent with the conclusions drawn earlier from the $\vec{\epsilon} \parallel [010]$ case: If sheets other than distorted ellipsoids of type B were involved in the observed oscil-

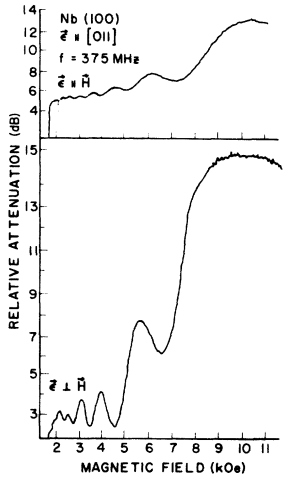

FIG. 9. Nb (100) magnetoacoustics: α_N vs H for $\vec{\epsilon} \parallel [011] \parallel \vec{H}$ (upper curve), and $\vec{\epsilon} \parallel [011] \perp \vec{H}$ (lower curve).

TABLE II. Δk theoretical and experimental values for Nb (100), $\vec{\epsilon} \parallel [011]$. Δk is given in units of Å^{-1}.

	Theory				Experiment	
1	2	3	4	5		
$(\vec{H}, \vec{\epsilon})$	$\hat{\epsilon} \cdot \hat{v}_F{}^2$ (IV and VI)	Δk	$(\epsilon \cdot v_F)^2$ (III and V)	Δk	Δk	mixing
0°	0.1	1.03 Å^{-1}	0.1	1.03 Å^{-1}	1.04 Å^{-1}	little
10°	0.0	1.08	0.2	0.98		
20°	0.0	1.13	0.2	0.96		
30°	0.1	1.20	0.3	0.95		
40°	0.2	1.24	0.4	0.94		
50°	0.8	1.24	0.6	0.94		
60°	0.9	1.20	0.7	0.95		
70°	1.0	1.13	0.8	0.96		
80°	1.0	1.08	0.8	0.98		
90°	0.9	1.03	0.9	1.03	1.05	little

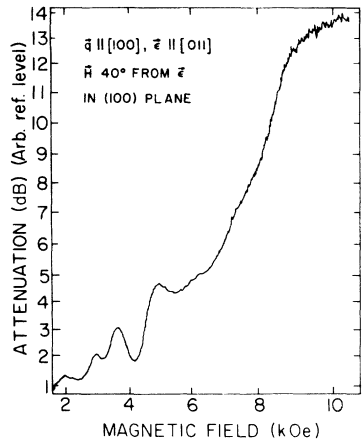

FIG. 10. Nb (100) magnetoacoustics: α_N vs H for $\vec{\epsilon} \parallel [011]$ and $\vec{H}$ 40° from $\vec{\epsilon}$ in (100) plane.

lations, the caliper degeneracy seen in Fig. 9—and for no other $\vec{H}$ orientations (cf. Fig. 10)—would not be expected. It is of course important, too, that the degenerate Δk value determined experimentally is about that expected from theory.

CONCLUSIONS

In summary, the evidence suggests that the shear polarization orientation can exert an important "weighting" effect on the MA interaction. Through its influence on oscillation amplitude, as measured roughly by $(\hat{\epsilon} \cdot v_F)^2$, the transverse-wave MA interaction can be far more selective among the available calipers (for given $\vec{H}$ orientation) than can the longitudinal. For the latter interaction the factors determining amplitude of the nth oscillation are essentially as given in the coefficient of Eq. (1). We have found that the polarization orientation can, as in the case $\vec{q} \parallel (100)$, $\vec{\epsilon} \parallel (010)$ of niobium, cause the transverse-wave MA interaction to be so selective that the calipers associated with a single Fermi sheet in Nb are swept out as $\vec{H}$ is rotated in the plane normal to $\vec{q}$.

What of the missing momenta from sheets other than distorted ellipsoids of type B? It could be argued that the momenta corresponding to the jungle gym and octahedron are missing as a consequence of interband scattering, since these sheets have points of degeneracy in $\vec{k}$ space. In the case of the octahedron a further contributing factor could be the relatively large curvatures at caliper end points. However, the absence of the type-A ellipsoids is much more difficult to account for, and we make the following speculation. Pippard[5] has pointed out that the shear-deformation interaction [corresponding to the π_1 force of Eq. (4a)] does not contribute on the effective zone when the latter coincides with a plane of mirror symmetry of the Fermi surface. This symmetry condition applies to the type-A ellipsoids but not to those of type B. (It also applies in the case of the jungle gym and octahedron.) Since the symmetry restriction does not apply to the electromagnetic interaction [associated with the force F_E, in Eq. (4)], the contribution of the latter to the attenuation might be expected to be qualitatively similar for the type-A and -B ellipsoids.

It would seem very speculative to conclude that, therefore, the electromagnetic interaction is not contributing. However, we have found other evidence in niobium to support just that contention:[13] We have found the so-called rapid-fall region in the zero-field shear-wave superconducting attenuation at T_c to be absent for $ql \gg 1$; further support comes from the properties of a maximum which we have found in the temperature dependence of the normal-state attenuation of niobium. These matters are not central to the present subject, however, and are treated elsewhere.[14]

ACKNOWLEDGMENTS

We wish to thank Dr. Richard Reed of Oak Ridge National Laboratory for the niobium samples, and Dr. T. Francavilla and Dr. J. R. Peverley for assistance in taking data. We wish also to thank E. Donovan for help in construction of some of the effective-zone projections.

[1] J. R. Leibowitz, E. Alexander, G. Blessing, T. Francavilla, and J. R. Peverley, *Low Temperature Physics LT*13, Boulder, Colorado, 1972, edited by W. J. O. Sullivan, K. D. Timmerhaus, and E. F. Hammel (Plenum, New York, 1974), Vol. 4.

[2] J. R. Leibowitz, J. R. Peverley, and E. Alexander, Phys. Lett. A 44, 298 (1973).

[3] L. R. Mattheiss, Phys. Rev. B 1, 373 (1970).

[4]J. Mertsching, Phys. Status Solidi 37, 465 (1970).
[5]A. B. Pippard, Proc. R. Soc. A 257, 165 (1960).
[6]G. B. Scott and M. Springford, Proc. R. Soc. A 320, 115 (1970).
[7]M. H. Halloran, J. H. Condon, J. E. Graebner, J. E. Kunzler, and F. S. L. Hsu, Phys. Rev. B 1, 366 (1970).
[8]We are indebted to J. R. Peverley for this argument.
[9]J. D. Gavenda and W. Royall Cox, Phys. Rev. B 6, 4392 (1972).
[10]D. S. Khatri and J. R. Peverley, Phys. Rev. Lett. 30, 490 (1973).
[11]T. Kjeldaas, Jr. and T. Holstein, Phys. Rev. Lett. 2, 340 (1959).
[12]M. H. Cohen, M. J. Harrison, and W. A. Harrison, Phys. Rev. 117, 937 (1960).
[13]J. R. Leibowitz, E. Alexander, G. Blessing, and T. Francavilla, in Vol. 3 of Ref. 1.
[14]Reference 13 outlines those results. A more detailed development is in preparation.

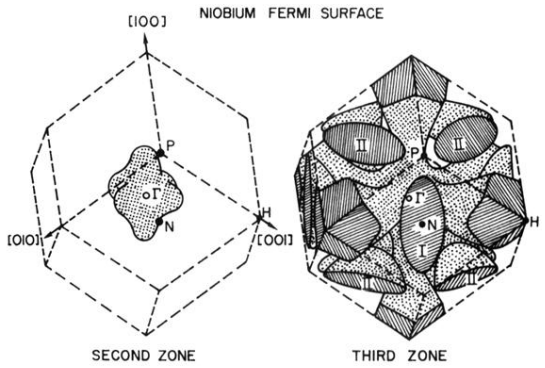

FIG. 1. Hole sheets of the Fermi surface in the second and third Brillouin zones of niobium [after Mattheiss (Ref. 3)].